

Spin-gap phase in nearly-half-filled one-dimensional conductors coupled with phonons

K. Yonemitsu*

Department of Applied Physics, Tohoku University, Sendai 980, Japan

M. Imada

Institute for Solid State Physics, University of Tokyo, Tokyo 106, Japan

(October 22, 2018)

Asymptotic properties of nearly-half-filled one-dimensional conductors coupled with phonons are studied through a renormalization group method. Due to spin-charge coupling via electron-phonon interaction, the spin correlation varies with filling as well as the charge correlation. Depending on the relation between cut-off energy scales of the Umklapp process and of the electron-phonon interaction, various phases appear. We found a metallic phase with a spin gap and a dominant charge-density-wave correlation near half filling between a gapless density-wave phase (like in the doped repulsive Hubbard model) and a superconductor phase with a spin gap. The spin gap is produced by phonon-assisted backward scatterings which are interfered with the Umklapp process constructively or destructively depending on the character of electron-phonon coupling.

72.15.Nj, 71.38.+i, 71.45.Lr, 71.30.+h

I. INTRODUCTION

Metallic states of doped copper oxides and related materials are extensively studied to clarify the characteristics of strongly correlated electron systems. The “spin gap” feature of the underdoped compounds [1] is one of the most peculiar features of them, but its origin is not yet clear. In a model with strong on-site attraction, there would be a temperature range in which local singlet pairs are formed with finite binding energy but the system is still not superconducting. In the case of the strong on-site repulsion, however, the spin gap formation must be the consequence of a subtle balance. As a fundamental property of strongly correlated materials, it is worth investigating the spin excitation gap in metals from various points of view. It is pointed out that a spin gap may play an important role both in determining the type of a metal-insulator transition [2] and in the mechanism of the high- T_c superconductivity. [3]

It has been pointed out that electron-phonon interaction can drastically change *local* quasiparticle characters of nearly-half-filled electron systems *when the on-site repulsion is strong*. [4–6] In this paper, we investigate asymptotic behaviors of correlation functions by integrating out short-distance degrees of freedom in space and time. Repulsive interaction and retarded attraction mediated by phonons are treated on an equal footing. Our studies are limited here to one dimension where a bosonization technique [7,8] can be used to derive renormalization group equations and to take the filling factor explicitly into account. Attention is paid to tendency for the formation of a spin gap near half filling and connections to the insulator phase at half filling and to a possible superconductor phase away from half filling.

Without electron-phonon interaction, spin and charge excitations are separated through bosonization which only describes low-energy excitations. Phonons couple with both spin and charge so that they are interfered with each other until electron-phonon interaction is integrated out at energy of the order of phonon frequency. This spin-charge coupling at finite energy leads the spin and charge correlations to depend on each other. Technically, it leads the equivalent two-dimensional classical system to have interacting Burgers vectors. [9]

At half filling, the Umklapp process tends to open a charge gap. Away from half filling, as the energy scale is made smaller, the Umklapp process becomes ineffective at finite energy which vanishes in the limit of half filling. Therefore the charge excitation is always gapless except half filling. Nevertheless the Umklapp process at finite energy modifies the charge correlation and also the spin correlation through the electron-phonon coupling. Thus the spin excitation is controlled by the relation between the cut-off energy scale of the Umklapp process and that of electron-phonon interaction. In terms of two-dimensional classical systems, the interactions between Burgers vectors originating from these two processes have different shapes and different length scales so that they are cut off in different manners. We numerically solve renormalization group equations for the correlation exponents and scattering parameters (fugacities in the classical system) and find a new phase which is made possible by both of these two processes.

In this paper, we study a bosonized Hamiltonian in which the standard electronic part is coupled with dispersionless phonons so that back and forward scatterings occur exchanging phonons as well as directly between electrons. In the electronic part, we consider on-site repulsion. The scattering parameters of electron-electron interaction are taken from the lowest-order perturbation with respect to on-site repulsion. This is because the exactly known, fixed-point

values of the pure Hubbard model [10] are no longer valid due to modified scaling properties. For a phonon-assisted backward scattering, we take a continuum version of the on-site Holstein coupling [11] or that of the intersite Su-Schrieffer-Heeger (SSH) coupling. [12] Furthermore, we add a phonon-assisted forward scattering which appears in the continuum version of the Holstein model in order to make a singlet superconductor phase possible. It is numerically confirmed that this addition to the SSH case does not affect the spin correlation so much.

The renormalization group equations we obtain deal with the lowest-order perturbations, so that the fixed point of either correlation exponent at zero should correspond to the Luther-Emery state [13] with a gap in the corresponding channel. At half filling, our results for the critical coupling strengths for the Holstein model and the SSH model (without a phonon-assisted forward scattering) to have a charge density wave with both spin and charge gaps are consistent with the critical coupling strengths for dimerization obtained analytically and by the quantum Monte Carlo method. [14] Away from half filling, the lattice is not statically distorted for purely one-dimensional phonons with finite frequency. More realistically, three-dimensionality of the crystal lattice would effectively freeze a periodic lattice distortion, if any. In this paper, we do not consider such a case but study effects of *dynamical* phonons on the spin excitation gap in correlated metals.

Far away from half filling where the Umklapp process is ineffective, a phase diagram is divided basically into a gapless phase with a dominant density-wave correlation as in the doped repulsive Hubbard model and a singlet superconductor phase with a spin gap for large enough electron-phonon interaction. Near half filling, we found a phase with a spin gap and a dominant charge-density-wave correlation between the two phases and call it a spin-gap charge-density-wave (SG-CDW) phase. This phase does not have a charge gap and is metallic with a finite Drude weight. The wave number of the SG-CDW is incommensurate to the lattice so that it should be metallic due to a phason mode. [15] The appearance of the SG-CDW phase is thus reasonable and related to the similar phase in Ref. [9] where an Umklapp process and a phonon-assisted forward scattering are not considered. In this paper, we clarify its relation with the Mott insulator phase and with a superconductor phase by treating both electron-electron and electron-phonon interactions at and away from half filling. Furthermore, effects of the combination of these two kinds of interactions near half filling are demonstrated to depend strongly on the form of electron-phonon interaction. It is reminiscent of the two-dimensional case [4] in that a system with strong on-site repulsion is more sensitive to an intersite electron-phonon coupling than an on-site one for a small phonon frequency.

This paper is organized as follows: Sec. II introduces the bosonized model. Relations of electron-phonon parameters to the g -ology parameters are examined. Sec. III outlines the derivation of renormalization group equations. Some modifications to previous works are described. It is confirmed that the antiadiabatic limit is correctly reproduced. Sec. IV shows phase diagrams for different electron-phonon couplings and phonon frequencies. The evolution of parameters with changing scales is demonstrated for typical examples to clarify the roles played by different processes. Sec. V summarizes the present work. Part of the results presented in this paper were reported briefly elsewhere. [16]

II. MODEL

We consider a Tomonaga-Luttinger model extended to include the spin and charge degrees of freedom, a backward scattering, an Umklapp process, and phonon-assisted back and forward scatterings. The electronic part is a standard one. [7,8] Assuming weak interactions, one can linearize the electronic dispersion relation around the Fermi points. The kinetic part is written as a term bilinear in boson operators for spin and charge densities,

$$\sigma_j(p) = \frac{1}{\sqrt{2}} (\rho_{j\uparrow}(p) - \rho_{j\downarrow}(p)) , \quad (2.1)$$

$$\rho_j(p) = \frac{1}{\sqrt{2}} (\rho_{j\uparrow}(p) + \rho_{j\downarrow}(p)) , \quad (2.2)$$

respectively, with the Fourier components of the electron density operators,

$$\rho_{j,s}(p) = \sum_k c_{j,k+p,s}^\dagger c_{j,k,s} , \quad (2.3)$$

for right ($j=1$) and left ($j=2$) movers with spin s . They obey commutation relations,

$$[\nu_1(-p), \nu_1(p')] = [\nu_2(p), \nu_2(-p')] = \frac{pL}{2\pi} \delta_{p,p'} , \quad (\nu = \sigma, \rho) . \quad (2.4)$$

A backward scattering between parallel spins ($g_{1\parallel}$), a forward scattering which couples the two branches, $j = 1, 2$, ($g_2 \equiv g_{2\parallel} = g_{2\perp}$), and a forward scattering within a single branch ($g_4 \equiv g_{4\perp}$, $g_{4\parallel}$ is set at zero.) are also written as bilinear terms. By combining them with the kinetic part, the spin and charge parts of the bilinear terms read

$$H_{\sigma,0} = \frac{2\pi v_F - g_4}{L} \sum_{p>0} [\sigma_1(p)\sigma_1(-p) + \sigma_2(-p)\sigma_2(p)] - \frac{g_{1\parallel}}{L} \sum_{p>0} [\sigma_1(p)\sigma_2(-p) + \sigma_1(-p)\sigma_2(p)] , \quad (2.5)$$

$$H_{\rho,0} = \frac{2\pi v_F + g_4}{L} \sum_{p>0} [\rho_1(p)\rho_1(-p) + \rho_2(-p)\rho_2(p)] - \frac{g_{1\parallel} - 2g_2}{L} \sum_{p>0} [\rho_1(p)\rho_2(-p) + \rho_1(-p)\rho_2(p)] , \quad (2.6)$$

respectively, where v_F is the Fermi velocity.

The other g processes are written with the help of the boson representation of the right-going ($j = 1$) and left-going ($j = 2$) electron fields with spin s ($s = \pm 1$),

$$\psi_{js}(x) = \lim_{\alpha \rightarrow 0} \frac{1}{\sqrt{2\pi\alpha}} \exp \left[\pm i k_F x \mp i \frac{1}{\sqrt{2}} (\phi_\rho(x) + s\phi_\sigma(x)) + i \frac{1}{\sqrt{2}} (\theta_\rho(x) + s\theta_\sigma(x)) \right] , \quad \text{for } j = \begin{cases} 1 \\ 2 \end{cases} , \quad (2.7)$$

where α is a cut-off parameter, k_F is the Fermi wave number, $\phi_\nu(x)$ and $\theta_\nu(x)$, ($\nu = \sigma, \rho$), are the fields defined as

$$\left. \begin{matrix} \phi_\nu(x) \\ \theta_\nu(x) \end{matrix} \right\} = \mp \frac{i\pi}{L} \sum_{p(\neq 0)} \frac{1}{p} e^{-\alpha|p|/2 - ipx} [\nu_1(p) \pm \nu_2(p)] . \quad (2.8)$$

The field $\Pi_\nu(x)$ defined as $\Pi_\nu(x) = \frac{1}{\pi} \partial_x \theta_\nu(x)$ is conjugate to the phase field $\phi_\nu(x)$,

$$[\phi_\nu(x), \Pi_\mu(y)] = i\delta_{\nu,\mu} \delta(x - y) . \quad (2.9)$$

With no magnetic field and at half filling, a backward scattering between antiparallel spins ($g_{1\perp}$) and an Umklapp process (g_3) read

$$\begin{aligned} H_{\sigma,\text{int}} &= g_{1\perp} \sum_s \int dx \psi_{1,s}^\dagger(x) \psi_{2,-s}^\dagger(x) \psi_{1,-s}(x) \psi_{2,s}(x) \\ &= \frac{2g_{1\perp}}{(2\pi\alpha)^2} \int dx \cos(2\sqrt{2}\phi_\sigma(x)) , \end{aligned} \quad (2.10)$$

$$\begin{aligned} H_{\rho,\text{int}} &= g_3 \int dx \left(\psi_{1,\uparrow}^\dagger(x) \psi_{1,\downarrow}^\dagger(x) \psi_{2,\downarrow}(x) \psi_{2,\uparrow}(x) + \text{h.c.} \right) \\ &= \frac{2g_3}{(2\pi\alpha)^2} \int dx \cos(2\sqrt{2}\phi_\rho(x)) , \end{aligned} \quad (2.11)$$

respectively. The bilinear terms are rewritten with the fields $\phi_\nu(x)$ and $\theta_\nu(x)$ as

$$H_{\nu,0} = \int \frac{dx}{2\pi} \left[u_\nu K_\nu (\partial_x \theta_\nu(x))^2 + \frac{u_\nu}{K_\nu} (\partial_x \phi_\nu(x))^2 \right] , \quad (2.12)$$

with velocities,

$$u_\sigma^2 = \left(v_F - \frac{g_4}{2\pi} \right)^2 - \left(\frac{g_{1\parallel}}{2\pi} \right)^2 , \quad (2.13a)$$

$$u_\rho^2 = \left(v_F + \frac{g_4}{2\pi} \right)^2 - \left(\frac{g_{1\parallel} - 2g_2}{2\pi} \right)^2 , \quad (2.13b)$$

and correlation exponents,

$$K_\sigma^2 = \frac{2\pi v_F - g_4 + g_{1\parallel}}{2\pi v_F - g_4 - g_{1\parallel}} , \quad (2.14a)$$

$$K_\rho^2 = \frac{2\pi v_F + g_4 + g_{1\parallel} - 2g_2}{2\pi v_F + g_4 - g_{1\parallel} + 2g_2} . \quad (2.14b)$$

With a magnetic field h or away from half filling, we add

$$h \int dx \frac{\sqrt{2}}{\pi} \partial_x \phi_\sigma(x) + \mu \int dx \frac{\sqrt{2}}{\pi} \partial_x \phi_\rho(x) , \quad (2.15)$$

where μ is the chemical potential set to be zero at half filling. In order to work with fixed magnetization (m) and filling (δn), where $m = \pm 1$ at saturated magnetization, $\delta n = 0$ at half filling, and $\delta n = 1$ at complete filling, Legendre transforms are performed. [17] Defining

$$\psi_\sigma(x) = \phi_\sigma(x) + \frac{\pi}{\sqrt{2}} m x , \quad (2.16a)$$

$$\psi_\rho(x) = \phi_\rho(x) + \frac{\pi}{\sqrt{2}} \delta n x , \quad (2.16b)$$

and rewriting $\psi_\sigma(x)$ and $\psi_\rho(x)$ as $\phi_\sigma(x)$ and $\phi_\rho(x)$, respectively, we get the electronic part of the model. The spin part,

$$H_\sigma = H_{0,\sigma} + H_{1\perp} , \quad (2.17)$$

consists of the “noninteracting” part,

$$H_{0,\sigma} = \int \frac{dx}{2\pi} \left[u_\sigma K_\sigma (\partial_x \theta_\sigma(x))^2 + \frac{u_\sigma}{K_\sigma} (\partial_x \phi_\sigma(x))^2 + \frac{\pi^2 u_\sigma m^2}{2K_\sigma} \right] , \quad (2.18)$$

and the perturbation due to the backward scattering,

$$H_{1\perp} = \frac{2g_{1\perp}}{(2\pi\alpha)^2} \int dx \cos(2\sqrt{2}\phi_\sigma(x) - 2\pi m x) , \quad (2.19)$$

while the charge part,

$$H_\rho = H_{0,\rho} + H_3 , \quad (2.20)$$

consists of the “noninteracting” part,

$$H_{0,\rho} = \int \frac{dx}{2\pi} \left[u_\rho K_\rho (\partial_x \theta_\rho(x))^2 + \frac{u_\rho}{K_\rho} (\partial_x \phi_\rho(x))^2 + \frac{\pi^2 u_\rho \delta n^2}{2K_\rho} \right] , \quad (2.21)$$

and the perturbation due to the Umklapp process,

$$H_3 = \frac{2g_3}{(2\pi\alpha)^2} \int dx \cos(2\sqrt{2}\phi_\rho(x) - 2\pi \delta n x) . \quad (2.22)$$

Here, we do not take the filling dependence of the Fermi velocity into account. In the lowest-order perturbation, the Hubbard model with the on-site interaction U corresponds to $g_{1\parallel} = g_{1\perp} = g_2 = g_3 = g_4 = U$. [8]

The phonon field is decomposed into a part with momenta near zero, $\phi_0(p)$, and the rest with momenta near π (in units of the inverse lattice spacing), $\phi_\pi(x)$. The former causes a forward scattering and is represented in the momentum space. The latter causes a backward scattering and is represented in the coordinate space. This decomposition is therefore made possible by the decomposition of the electron field into the right- and left-going ones so that it is achieved unambiguously. Their conjugate momenta are denoted by $\Pi_0(p)$ and $\Pi_\pi(x)$, respectively.

$$[\phi_0(p), \Pi_0(q)] = i\delta_{p,q} , \quad (2.23)$$

$$[\phi_\pi(x), \Pi_\pi(y)] = i\delta(x - y) . \quad (2.24)$$

Note that $\phi_\pi(x)$ and $\Pi_\pi(x)$ are real fields.

In the phonon part, we take dispersionless phonons for simplicity. Later we will consider electron-phonon couplings in the Holstein model and in the SSH model when evaluating correlation exponents. The neglect of the dispersion of bare phonons is not essential since it is absent in the former model and the acoustic phonons are decoupled from the low-energy electronic spectrum in the continuum limit of the latter model. [14] We divide the phonon part into a part with momenta near π and the rest with momenta near zero,

$$H_{\text{ph}} = \frac{1}{2} \int dx [\Pi_{\pi}^2(x) + \omega_{\pi}^2 \phi_{\pi}^2(x)] + \frac{1}{2L} \sum_p [|\Pi_0(p)|^2 + \omega_0^2 |\phi_0(p)|^2] , \quad (2.25)$$

where ω_{π} and ω_0 are their respective phonon frequencies.

The Holstein coupling to the dispersionless phonons is represented by

$$\sum_i \left(\beta q_i n_i + \frac{K}{2} q_i^2 + \frac{1}{2M} p_i^2 \right) , \quad (2.26)$$

with the electron density at site i , n_i , the lattice displacement q_i , its conjugate momentum p_i , the coupling strength β , the spring constant K , and the ionic mass M . In the continuum limit, it can be written as $H_1 + H_2 + H_{\text{ph}}$, where H_1 denotes a phonon-assisted backward scattering,

$$H_1 = \gamma_1 \sum_s \int dx \left[\psi_{2,s}^{\dagger}(x) \psi_{1,s}(x) e^{i\pi\delta n x} + \psi_{1,s}^{\dagger}(x) \psi_{2,s}(x) e^{-i\pi\delta n x} \right] \phi_{\pi}(x) , \quad (2.27)$$

and H_2 stands for a phonon-assisted forward scattering,

$$H_2 = \gamma_2 \frac{\sqrt{2}}{L} \sum_p [\rho_1(-p) + \rho_2(-p)] \phi_0(p) , \quad (2.28)$$

with $\gamma_1 = \gamma_2 = \beta/\sqrt{M}$ and $\omega_{\pi} = \omega_0 = \sqrt{K/M}$. Note that the operators $\psi_{1,s}(x)$, $\psi_{2,s}(x)$, and $\phi_{\pi}(x)$ above concern with the slowly varying part, whereas the rapidly oscillating parts give the factors $e^{\pm i\pi\delta n x} = e^{\pm i(2k_F - \pi)x}$.

The SSH coupling to the phonons is represented by

$$\sum_i \left[\alpha_s (q_{i+1} - q_i) \sum_s (c_{i,s}^{\dagger} c_{i+1,s} + c_{i+1,s}^{\dagger} c_{i,s}) + \frac{K}{2} (q_{i+1} - q_i)^2 + \frac{1}{2M} p_i^2 \right] , \quad (2.29)$$

with $c_{i,s}$ annihilating an electron with spin s at site i , α_s being the coupling strength, and q_i , p_i , K and M as above. In the continuum limit, by neglecting the phonon dispersion, it can be written as $H_{-1} + H_{\text{ph}}$, where H_{-1} denotes a phonon-assisted backward scattering,

$$H_{-1} = \gamma_{-1} \sum_s \int dx \left[i \psi_{2,s}^{\dagger}(x) \psi_{1,s}(x) e^{i\pi\delta n x} - i \psi_{1,s}^{\dagger}(x) \psi_{2,s}(x) e^{-i\pi\delta n x} \right] \phi_{\pi}(x) , \quad (2.30)$$

with $\gamma_{-1} = 4\alpha_s/\sqrt{M}$ and $\omega_{\pi} = 2\sqrt{K/M}$. The scatterings H_1 and H_{-1} differ in the form factor.

For later convenience, we define parameters X_{ν} depending only on K_{ν} and dimensionless coupling strengths Y_{ν} as [9]

$$X_{\nu} = 2(1 - K_{\nu}^{-1}) , \quad (2.31)$$

$$Y_{\sigma} = g_{1\perp}/(\pi v_F) , \quad (2.32a)$$

$$Y_{\rho} = g_3/(\pi v_F) . \quad (2.32b)$$

In the lowest order, the parameters X_{σ} and X_{ρ} are given by

$$X_{\sigma} \simeq g_{1\parallel}/(\pi v_F) , \quad (2.33a)$$

$$X_{\rho} \simeq (g_{1\parallel} - 2g_2)/(\pi v_F) , \quad (2.33b)$$

respectively. Hereafter, the Hubbard model is meant for $H_H = H_\sigma + H_\rho$ with $X_\sigma = Y_\sigma = -X_\rho = Y_\rho \equiv Y_{\text{el}} = U/(\pi v_F) > 0$, the Holstein-Hubbard model for $H_{H-H} = H_H + H_{\text{ph}} + H_1 + H_2$ with $\omega_\pi = \omega_0 \equiv \omega = \sqrt{K/M}$ and $\gamma_1 = \gamma_2 = \beta/\sqrt{M}$, and the SSH-Hubbard model for $H_{\text{SSH-H}} = H_H + H_{\text{ph}} + H_{-1}$ with $\omega_\pi \equiv \omega = 2\sqrt{K/M}$ and $\gamma_{-1} = 4\alpha_s/\sqrt{M}$. Numerical evaluations are performed also in the SSH-Hubbard model supplemented with a forward scattering, $H_{\text{SSH-H-f.s.}} = H_{\text{SSH-H}} + H_2$, with $\omega_0 = \omega_\pi$ and $\gamma_2 = \gamma_{-1}$.

Effective interactions are obtained through the integration of phonon fields. First we consider the antiadiabatic limit ($\omega \rightarrow \infty$), where the interactions are instantaneous. In this limit, Eq. (2.26) becomes

$$-\frac{\beta^2}{K} \sum_i c_{i\uparrow}^\dagger c_{i\uparrow} c_{i\downarrow}^\dagger c_{i\downarrow}, \quad (2.34)$$

which corresponds to $g_{1\parallel} = g_{1\perp} = g_2 = g_3 = g_4 = -\beta^2/K$, and Eq. (2.29) becomes

$$-\frac{\alpha_s^2}{2K} \sum_{i,s,s'} (c_{i,s}^\dagger c_{i+1,s} + c_{i+1,s}^\dagger c_{i,s}) (c_{i,s'}^\dagger c_{i+1,s'} + c_{i+1,s'}^\dagger c_{i,s'}) , \quad (2.35)$$

which corresponds to $g_{1\parallel} = g_{1\perp} = -g_3 = -4\alpha_s^2/K$ and $g_2 = g_4 = 0$. Later we will take either a phonon-assisted backward scattering originating from the on-site coupling (γ_1) or that from the intersite coupling (γ_{-1}), but not both. We then define a dimensionless coupling strength Y_1 as

$$Y_1 = \frac{\gamma_{\pm 1}^2}{\pi v_F \omega_\pi^2}. \quad (2.36)$$

If necessary, the two cases above are distinguished by $f = 1$ for γ_1 and $f = -1$ for γ_{-1} . Another dimensionless coupling strength Y_2 is defined as

$$Y_2 = \frac{\gamma_2^2}{\pi v_F \omega_0^2}. \quad (2.37)$$

The subscripts of Y_1 and Y_2 stand for back and forward scatterings, respectively, as those in g parameters. In the Holstein-Hubbard model and the SSH-Hubbard model supplemented with a forward scattering, we define Y_{ph} as $Y_1 = Y_2 \equiv Y_{\text{ph}}$. Summarizing the antiadiabatic case, electron-phonon interaction shifts the electronic parameters by $X_\sigma \rightarrow X_\sigma - Y_1$, $Y_\sigma \rightarrow Y_\sigma - Y_1$, $X_\rho \rightarrow X_\rho - (Y_1 - 2Y_2)$, and $Y_\rho \rightarrow Y_\rho - fY_1$. From the definitions, (2.32a), (2.33a), and (2.33b), the first three are interpreted as due to effective attraction. The difference between the on-site coupling ($f = 1$) and the intersite coupling ($f = -1$) appears in the effect on Y_ρ . Its origin is easily understood in the continuum limit. The effective g_1 processes come from the contraction of $\psi_{2,s}^\dagger(x)\psi_{1,s}(x)$ and $\psi_{1,s'}^\dagger(x)\psi_{2,s'}(x)$ in H_1 or H_{-1} , whereas the effective g_3 processes come from the contraction of $\psi_{2,s}^\dagger(x)\psi_{1,s}(x)$ and $\psi_{2,-s}^\dagger(x)\psi_{1,-s}(x)$ and that of $\psi_{1,s}^\dagger(x)\psi_{2,s}(x)$ and $\psi_{1,-s}^\dagger(x)\psi_{2,-s}(x)$, giving the sign factor f . Hereafter, we will not consider a g_4 process, which only yields a renormalization of the Fermi velocity.

To treat finite phonon frequencies, we consider the partition function $Z = \text{Tr} e^{-\beta H}$ at the inverse temperature β and map the present system to a two-dimensional classical system in the Euclidean space $\mathbf{r} = (x, y = v_F \tau)$ with an imaginary time τ . [9] Because the phonon fields are bilinear in the Hamiltonian, they are analytically integrated out. Effective interactions $H_{i,\text{eff}}$ ($i = \pm 1, 2$) are defined as

$$\text{T}_\tau \exp \left[- \int_0^\beta d\tau H_{i,\text{eff}}(\tau) \right] = \left\langle \text{T}_\tau \exp \left[- \int_0^\beta d\tau H_i(\tau) \right] \right\rangle_{\text{ph}}, \quad (2.38)$$

where T_τ is the time-ordering operator in the imaginary time, and $\langle \cdots \rangle_{\text{ph}}$ denotes an expectation value averaged over phonon fields. It is straightforward to derive, in the $\beta \rightarrow \infty$ limit,

$$H_{1,\text{eff}}(\tau) = -\frac{\gamma_1^2}{\omega_\pi^2 (2\pi\alpha)^2} \sum_{\epsilon_1=\pm 1} \int dx \int d\Delta\tau \left[\frac{\omega_\pi}{2} e^{-\omega_\pi |\Delta\tau|} \right] \frac{1}{2} \sum_{\epsilon_2, \epsilon'_1, \epsilon'_2=\pm 1} \exp \left\{ i\epsilon_1 \left(\sqrt{2}\phi_\sigma(1) - \pi m x \right) \right. \\ \left. - i\epsilon_2 \left(\sqrt{2}\phi_\sigma(2) - \pi m x \right) + i\epsilon'_1 \left(\sqrt{2}\phi_\rho(1) - \pi \delta n x \right) - i\epsilon'_2 \left(\sqrt{2}\phi_\rho(2) - \pi \delta n x \right) \right\}, \quad (2.39)$$

$$H_{2,\text{eff}}(\tau) = -\frac{2\gamma_2^2}{\omega_0^2} \frac{1}{L} \sum_{p>0} \int d\Delta\tau \left[\frac{\omega_0}{2} e^{-\omega_0 |\Delta\tau|} \right] \{ \rho_1(p, \tau_1) + \rho_2(p, \tau_1) \} \{ \rho_1(-p, \tau_2) + \rho_2(-p, \tau_2) \}, \quad (2.40)$$

$$H_{-1,\text{eff}}(\tau) = -\frac{\gamma_{-1}^2}{\omega_\pi^2(2\pi\alpha)^2} \sum_{\epsilon_1=\pm 1} \int dx \int d\Delta\tau \left[\frac{\omega_\pi}{2} e^{-\omega_\pi|\Delta\tau|} \right] \frac{1}{2} \sum_{\epsilon_2, \epsilon'_1, \epsilon'_2=\pm 1} \text{sgn}(\epsilon'_1\epsilon'_2) \exp \left\{ i\epsilon_1 \left(\sqrt{2}\phi_\sigma(1) - \pi m x \right) \right. \\ \left. - i\epsilon_2 \left(\sqrt{2}\phi_\sigma(2) - \pi m x \right) + i\epsilon'_1 \left(\sqrt{2}\phi_\rho(1) - \pi \delta n x \right) - i\epsilon'_2 \left(\sqrt{2}\phi_\rho(2) - \pi \delta n x \right) \right\}, \quad (2.41)$$

where arguments 1 and 2 denote $(x, v_F\tau_1)$ and $(x, v_F\tau_2)$, respectively, $\tau = (\tau_1 + \tau_2)/2$, and $\Delta\tau = \tau_1 - \tau_2$. In the $\omega \rightarrow \infty$ limit, $[\dots]$ above becomes $\delta(\tau_1 - \tau_2)$ so that the $\epsilon_1\epsilon_2 = \epsilon'_1\epsilon'_2 = 1$ terms in Eqs. (2.39) and (2.41) correspond to the $g_{1\parallel}$ process, $-\epsilon_1\epsilon_2 = \epsilon'_1\epsilon'_2 = 1$ to the $g_{1\perp}$ process, $\epsilon_1\epsilon_2 = -\epsilon'_1\epsilon'_2 = 1$ to the $g_3(=g_{3\perp})$ process, and $-\epsilon_1\epsilon_2 = -\epsilon'_1\epsilon'_2 = 1$ to the $g_{3\parallel}$ process not considered here, whereas the cross terms in Eq. (2.40) correspond to the $g_2(=g_{2\parallel}=g_{2\perp})$ processes, and the rest to the $g_{4\parallel}=g_{4\perp}$ processes. Note that $\mp g_4 = \mp g_{4\perp}$ in Eqs. (2.5) and (2.6) are replaced by $g_{4\parallel} \mp g_{4\perp}$ if $g_{4\parallel} \neq 0$. Again, we can derive $X_\sigma \rightarrow X_\sigma - Y_1$, $Y_\sigma \rightarrow Y_\sigma - Y_1$, $X_\rho \rightarrow X_\rho - (Y_1 - 2Y_2)$, and $Y_\rho \rightarrow Y_\rho - fY_1$ in this limit.

Finally, we have the “noninteracting” part, $H_0 = H_{0,\sigma} + H_{0,\rho}$, and perturbations, $H_{1\perp}$, H_3 , $H_{\pm 1,\text{eff}}(\tau)$, and $H_{2,\text{eff}}(\tau)$.

III. RENORMALIZATION EQUATIONS

Renormalization group equations are derived in a way similar to Voit-Schulz [9] and Giamarchi-Schulz [17]. Because of the similarity, we will not go into details but will give an outline detailed enough to explain a few modifications. We consider the correlation function,

$$R_\nu(\mathbf{r}_{12}) = \left\langle T_\tau e^{i\sqrt{2}\phi_\nu(\mathbf{r}_1)} e^{-i\sqrt{2}\phi_\nu(\mathbf{r}_2)} \right\rangle, \quad (3.1)$$

with $\mathbf{r}_{12} = \mathbf{r}_1 - \mathbf{r}_2$ and develop in powers of Y_σ , Y_ρ , Y_1 , and Y_2 . In the zeroth order, it is given by

$$R_\nu^{(0)}(\mathbf{r}_{12}) = \exp \left(-\frac{K_\nu}{2} \log \frac{r_{12}^2 + \alpha^2}{\alpha^2} \right). \quad (3.2)$$

In the expansion, we sum only over those configurations which satisfy the spin- and charge-conservation conditions: the sum of the coefficients of the ϕ_σ terms in the exponents and that of the ϕ_ρ terms are zero. Each term is written as a product of a spin part and a charge part the exponents of which are linear in ϕ_σ and ϕ_ρ , respectively, so that the expectation value is easily obtained. As a result, each term is written as an integral the variables of which can be regarded as positions of Burgers vectors in the Euclidean space [9] and denoted by \mathbf{r}_i , ($i = a, b, \dots$). The perturbation $H_{\pm 1,\text{eff}}(\tau)$ produces two vectors each of which is allowed to take one of four possible orientations $\pm \mathbf{b}_1$ and $\pm \mathbf{b}_2$ with $\mathbf{b}_{1,2} = (K_\sigma^{1/2}, \pm K_\rho^{1/2})$. The perturbation $H_{1\perp}$ produces a vector \mathbf{b}_σ or $-\mathbf{b}_\sigma$ with $\mathbf{b}_\sigma = (2K_\sigma^{1/2}, 0)$, while H_3 produces a vector \mathbf{b}_ρ or $-\mathbf{b}_\rho$ with $\mathbf{b}_\rho = (0, 2K_\rho^{1/2})$. The perturbation $H_{2,\text{eff}}(\tau)$ is represented with different operators and not interpreted as producing Burgers vectors: it will be treated later. For example, the $O(Y_\nu^2)$ term, ($\nu = \sigma, \rho$), is regarded as arising from a logarithmic interaction,

$$-\mathbf{b}(\mathbf{r}_a) \cdot \mathbf{b}(\mathbf{r}_b) \frac{1}{2} \log \frac{|\mathbf{r}_a - \mathbf{r}_b|^2 + \alpha^2}{\alpha^2}, \quad (3.3)$$

with $\mathbf{b}(\mathbf{r}_a) = -\mathbf{b}(\mathbf{r}_b) = \pm \mathbf{b}_\nu$ in a classical system of Burgers vectors if $m = 0$ and $\delta n = 0$. With $m \neq 0$ and $\delta n \neq 0$, the corresponding interaction becomes anisotropic in the Euclidean space. [17] The $O(Y_1)$ term corresponds to a contribution from a logarithmic plus linear potential,

$$-\mathbf{b}(\mathbf{r}_a) \cdot \mathbf{b}(\mathbf{r}_b) \frac{1}{2} \log \frac{|\mathbf{r}_a - \mathbf{r}_b|^2 + \alpha^2}{\alpha^2} - \frac{|y_a - y_b|}{\xi_\pi}, \quad (3.4)$$

with a constraint $x_a = x_b$, $\mathbf{b}(\mathbf{r}_a) = -\mathbf{b}(\mathbf{r}_b) = \pm \mathbf{b}_i$, ($i = 1, 2$), and $\xi_\pi = v_F/\omega_\pi$. The second term and the constraint come from the phonon propagator in Eqs. (2.39) and (2.41),

$$D_\pi(\mathbf{r}_a - \mathbf{r}_b) = \frac{1}{2\omega_\pi} \delta(x_a - x_b) \exp \left[-\frac{|y_a - y_b|}{\xi_\pi} \right], \quad (3.5)$$

which becomes isotropic in the antiadiabatic limit. The integral in each term is dominated by configurations with \mathbf{r}_a very close to \mathbf{r}_b . Then it is convenient to change the integration variables to $\mathbf{R} = (\mathbf{r}_a + \mathbf{r}_b)/2$ and $\mathbf{r} = \mathbf{r}_a - \mathbf{r}_b$ and

expand the integrand to the second order in \mathbf{r} . Integration can be performed over \mathbf{R} . [17] The remaining integration over \mathbf{r} is cut off at α ($r > \alpha$) and the function $\log[(r^2 + \alpha^2)/\alpha^2]/2$ is replaced by $\log(r/\alpha)$.

We will search a renormalized correlation function of the form,

$$\exp\left(-\frac{K_\nu^{\text{eff}}}{2} \log \frac{r_{12}^2 + \alpha^2}{\alpha^2} - d_\nu^{\text{eff}} \frac{x_{12}^2 - y_{12}^2}{r_{12}^2}\right), \quad (3.6)$$

regarding the corrections as modifying the exponent K_ν to an effective one K_ν^{eff} and producing the anisotropy parameter d_ν^{eff} . Changing the cut off α from $\alpha(l) \equiv \alpha e^l$ to $\alpha(l + dl)$, a pair of Burgers vectors with $\alpha(l) < r < \alpha(l + dl)$ are no more visible. This portion of the integrals can be absorbed into changing $K_\nu(l) [= 1/(1 - X_\nu(l)/2)]$ and $d_\nu(l)$ into $K_\nu(l + dl)$ and $d_\nu(l + dl)$. Upon rescaling the remaining integrals so that they again range from α to infinity, the effective parameters K_ν^{eff} and d_ν^{eff} are written with modified couplings $Y_\nu(l + dl)$ and $Y_1(l + dl)$. In addition, nonneutral pairs of Burgers vectors with $\alpha(l) < r < \alpha(l + dl)$ appearing in the $O(Y_\nu Y_1)$, $O(Y_1^2)$, $O(Y_\nu^2 Y_1)$ terms, etc., are combined into new vectors: \mathbf{b}_1 and \mathbf{b}_2 into \mathbf{b}_σ , \mathbf{b}_1 and $-\mathbf{b}_2$ into \mathbf{b}_ρ , \mathbf{b}_σ and $-\mathbf{b}_2(-\mathbf{b}_1)$ into $\mathbf{b}_1(\mathbf{b}_2)$, \mathbf{b}_ρ and $\mathbf{b}_2(-\mathbf{b}_1)$ into $\mathbf{b}_1(-\mathbf{b}_2)$, etc. They also contribute to modifying $Y_\nu(l)$ and $Y_1(l)$ into $Y_\nu(l + dl)$ and $Y_1(l + dl)$. The magnetic field h and the chemical potential μ are evaluated perturbationally. From the scaling $h(l) = e^l h$ and $\mu(l) = e^l \mu$, [17] we derive the relation between $m(l)$ and $m(l + dl)$ and that between $\delta n(l)$ and $\delta n(l + dl)$. The factors $e^{\pm i 2 \pi m x}$ in Eq. (2.19), $e^{\pm i 2 \pi \delta n x}$ in Eq. (2.22), and $(\omega_\pi/2)e^{-\omega_\pi |\Delta \tau|}$ in Eqs. (2.39) and (2.41) make the correlation functions anisotropic in the Euclidean space. A resultant change of the y scale relative to the x scale in $R_\nu(\mathbf{r}_{12})$ can be interpreted as a change of the velocity in the ν channel: $d[d_\nu(l)]/dl = -[K_\nu(l)/2]d\log[u_\nu(l)]/dl$ in the lowest order.

Finally, we obtain the renormalization group equations,

$$dX_\sigma(l)/dl = -Y_\sigma^2(l)J_0(2\pi m(l)\alpha) - Y_1(l)D_\pi(l), \quad (3.7)$$

$$dY_\sigma(l)/dl = -X_\sigma(l)Y_\sigma(l) - Y_1(l)D_\pi(l), \quad (3.8)$$

$$d(2\pi m(l)\alpha)/dl = 2\pi m(l)\alpha + Y_\sigma^2(l)J_1(2\pi m(l)\alpha), \quad (3.9)$$

$$d\log[u_\sigma(l)]/dl = -\frac{1}{2}K_\sigma(l) [Y_\sigma^2(l)J_2(2\pi m(l)\alpha) + Y_1(l)D_\pi(l)], \quad (3.10)$$

$$dX_\rho(l)/dl = -Y_\rho^2(l)J_0(2\pi \delta n(l)\alpha) - Y_1(l)D_\pi(l) + 2Y_2(l)D_0(l), \quad (3.11)$$

$$dY_\rho(l)/dl = -X_\rho(l)Y_\rho(l) - fY_1(l)D_\pi(l), \quad (3.12)$$

$$d(2\pi \delta n(l)\alpha)/dl = 2\pi \delta n(l)\alpha + Y_\rho^2(l)J_1(2\pi \delta n(l)\alpha), \quad (3.13)$$

$$d\log[u_\rho(l)]/dl = -\frac{1}{2}K_\rho(l) [Y_\rho^2(l)J_2(2\pi \delta n(l)\alpha) + Y_1(l)D_\pi(l)], \quad (3.14)$$

$$dY_1(l)/dl = [2 - K_\sigma(l) - K_\rho(l) - Y_\sigma(l)J_0(2\pi m(l)\alpha) - fY_\rho(l)J_0(2\pi \delta n(l)\alpha)] Y_1(l), \quad (3.15)$$

$$dY_2(l)/dl = 0, \quad (3.16)$$

where $D_\mu(l) = [\alpha(l)/\xi_\mu] \exp[-\alpha(l)/\xi_\mu]$, ($\mu = 0, \pi$). Since the cut-off parameter α should be physically of the order of k_F^{-1} , $D_\mu(l)$ can be regarded as $D_\mu(l) = [\omega_\mu/E(l)] \exp[-\omega_\mu/E(l)]$, with $E(l) = E_F e^{-l}$ and E_F being the Fermi energy. The $J_n(x)$ are the Bessel functions, whose oscillations spuriously come from the use of a sharp cut off in real space. In numerical integrations, we replace them by $J_n(x)\theta(j_{0,1} - |x|)$ with $j_{0,1}$ being the first zero of $J_0(x)$ [$J_0(j_{0,1}) = 0$], $\theta(x) = 1$ for $x > 0$ and $\theta(x) = 0$ for $x < 0$. The first terms in Eqs. (3.8) and (3.12) are linearized in X_ν since we deal with the lowest-order perturbations. In the absence of Y_1 and Y_2 , these equations are reduced to known ones. [7] Furthermore, they are consistent with the isotropy in spin space [$X_\sigma(l) = Y_\sigma(l)$ when $m = 0$]. The velocities u_ν would be modified also through Eqs. (2.13a) and (2.13b), but it is of higher order and neglected here. In the lowest order considered here, they are decoupled from the rest. Compared with the previous works [9,18], the factor e^l is absorbed

into the prefactor of $D_\mu(l)$ so that the right-hand sides of Eqs. (3.15) and (3.16) are not $(3 - \dots)Y_1(l)$ and $Y_2(l)$ any more, respectively. If the function $\langle T_\tau[\phi_\nu(\mathbf{r}_1) - \phi_\nu(\mathbf{r}_2)]^2 \rangle$ were renormalized as in Ref. [9], a factor of 2 would appear in the above equations. To keep the equations similar to those in the references, we doubled the definition of Y_1 . In Eq. (3.11), the effect of a phonon-assisted forward scattering is twice as large as that of a phonon-assisted backward scattering, as is expected from Eq. (2.33b), but it is not in Ref. [18]. As we show below, the present equations correctly reproduce the antiadiabatic limit discussed before.

To reproduce the antiadiabatic limit, we should recall that $\log[(r^2 + \alpha^2)/\alpha^2]/2$ was replaced above by $\log(r/\alpha)$ before the renormalization procedure. Because the largest electron-phonon contribution comes from $r \sim \xi_\mu$, ($\mu = 0, \pi$), it would be valid if α were much smaller than ξ_μ . However, a large value of ω_μ/E_F corresponds to a large value of α/ξ_μ , so that this replacement is no longer valid. Instead, we will derive the Y_1 and Y_2 terms in the equations for X_ν and Y_ν , ($\nu = \sigma, \rho$), in a more straightforward manner. Equations (2.39), (2.40), and (2.41) for the effective couplings $H_{i,\text{eff}}$, ($i = \pm 1, 2$), represent the electron-phonon contribution to the effective g parameters with a retardation factor $(\omega_\mu/2) \exp(-\omega_\mu |\Delta\tau|)$. As the time scale changes from $E(l)^{-1}$ to $E(l+dl)^{-1}$, the integration of the above factor over the time slice with width $E(l)^{-1}dl$ can be absorbed into definitions of the g parameters, for example, as

$$\begin{aligned} g_{1\parallel}(l+dl) &= g_{1\parallel}(l) - \frac{\gamma_{\pm 1}^2}{\omega_\pi^2} \left(\int_{-E(l+dl)^{-1}}^{-E(l)^{-1}} d\Delta\tau + \int_{E(l)^{-1}}^{E(l+dl)^{-1}} d\Delta\tau \right) \frac{\omega_\pi}{2} e^{-\omega_\pi |\Delta\tau|} \\ &= g_{1\parallel}(l) - \frac{\gamma_{\pm 1}^2}{\omega_\pi^2} D_\pi(l) dl, \end{aligned} \quad (3.17a)$$

and similarly as

$$g_{1\perp}(l+dl) = g_{1\perp}(l) - \frac{\gamma_{\pm 1}^2}{\omega_\pi^2} D_\pi(l) dl, \quad (3.17b)$$

$$g_3(l+dl) = g_3(l) - f \frac{\gamma_{\pm 1}^2}{\omega_\pi^2} D_\pi(l) dl, \quad (3.17c)$$

$$g_2(l+dl) = g_2(l) - \frac{\gamma_2^2}{\omega_0^2} D_0(l) dl, \quad (3.17d)$$

and an equation for $g_4(l+dl)$ similar to that for $g_2(l+dl)$. Note that here we do not take account of the effective g processes of the purely electronic origin. From these equations, the Y_1 terms are derived again and the Y_2 term is derived here. Since $H_{2,\text{eff}}(\tau)$ does not produce Burgers vectors, Y_2 is independent of the scale. It simply modifies $X_\rho(l)$ without interference with other quantities. Note that similar renormalization group equations can be derived with Feynman diagrams. Equations (3.15) and (3.16) are interpreted as originating from corrections to the electron-phonon vertices. The absence of a correction to the $Y_2(l)$ term is due to the fact that the bubble diagram in the zero-sound channel appearing in corrections to the phonon-assisted backward scattering gives the logarithmic correction [Eq. (3.15)] while that in the third channel appearing in corrections to the phonon-assisted forward scattering does not give a logarithmic correction [Eq. (3.16)]. [7]

Returning to the discussion of the antiadiabatic case, we should note that the variable l ranges from 0 to ∞ so that $E(l)$ from E_F to 0 in Eqs. (3.7), (3.8), (3.11), and (3.12). It corresponds to $E_F^{-1} < |\Delta\tau| < \infty$ in spite of unconstrained lattice dynamics at $0 < |\Delta\tau| < \infty$. This is in contrast to the purely electronic processes contributing to the effective g processes [the first terms in Eqs. (3.7), (3.8), (3.11), and (3.12)] and the corrections to the electron-phonon vertex [Eq. (3.15)], which are limited to $E_F > E(l) > 0$ [not included in Eqs. (3.17)]. Therefore, we integrate the second and third terms in Eqs. (3.7), (3.8), (3.11), and (3.12) over $-\infty < l < 0$ corresponding to $0 < |\Delta\tau| < E_F^{-1}$ with fixed values of Y_1 and Y_2 before integrating the renormalization group equations over $0 < l < \infty$. It leads us to choose the initial conditions as [18]

$$X_\sigma(0) = X_\sigma - Y_1 \left(1 - e^{-\omega_\pi/E_F} \right), \quad (3.18a)$$

$$Y_\sigma(0) = Y_\sigma - Y_1 \left(1 - e^{-\omega_\pi/E_F} \right), \quad (3.18b)$$

$$X_\rho(0) = X_\rho - Y_1 \left(1 - e^{-\omega_\pi/E_F} \right) + 2Y_2 \left(1 - e^{-\omega_0/E_F} \right), \quad (3.18c)$$

$$Y_\rho(0) = Y_\rho - fY_1 \left(1 - e^{-\omega_\pi/E_F}\right). \quad (3.18d)$$

In the antiadiabatic limit, the Y_1 and Y_2 terms are dropped from the renormalization group equations so that electron-phonon interaction simply shifts the initial conditions as discussed in Sec. II.

IV. RESULTS

First we consider analytic properties of the equations. The phonon propagator $D_\mu(l)$ has a maximum at $E(l) = \omega_\mu$ and decreases exponentially for $E(l) < \omega_\mu$. This smoothly cuts off the contribution from electron-phonon interaction at energy of the order of phonon frequency. Since Y_1 also changes exponentially, the actual cut off is different from ω_π . Except for unphysically strong, intersite electron-phonon coupling (in view of the fact that $\alpha_s(q_{i+1} - q_i)$ must be smaller than the bare transfer integral in the SSH model), $Y_1(l)D_\pi(l)$ finally decreases exponentially at large l as well as $Y_2(l)D_0(l)$. Then the Y_1 and Y_2 terms become negligible so that the equations for the spin part and for the charge part are decoupled to be in the familiar forms: effectively electron-phonon coupling is no more retarded and the system becomes equivalent to a purely electronic system with modified coupling strengths.

It should be noted that a spin-charge coupling at finite energy is a general phenomenon regardless of the presence of electron-phonon interaction: spin and charge are separated (in general only) asymptotically, i.e., in the limit of low energy and long wave length. Some purely electronic interaction may induce a filling dependence of the asymptotic spin correlation through a spin-charge coupling and an Umklapp process at finite energy. However, the Hubbard model is not the case since the fixed point of K_σ , K_σ^* , is known to be unity for $U > 0$ regardless of filling. Recall that, if both of the spin part and the charge part belong to the Tomonaga-Luttinger class, the charge-density-wave correlation is proportional to $r^{-K_\sigma^* - K_\rho^*}$, the spin-density-wave correlation to $r^{-K_\sigma^{*-1} - K_\rho^*}$, the singlet-superconductor correlation to $r^{-K_\sigma^* - K_\rho^{*-1}}$, and the triplet-superconductor correlation to $r^{-K_\sigma^{*-1} - K_\rho^{*-1}}$, in the asymptotic limit.

Deviation from half filling and nonzero magnetization, if any, grow exponentially with l . If a charge density wave is formed at half filling, charged solitons would be formed upon doping to connect two degenerate phases. The quantity $\delta n \alpha$ can be regarded as the expected number of charged solitons inside the length α . As the renormalization proceeds with increasing length scale and decreasing energy scale, the Umklapp process Y_ρ becomes ineffective at finite energy which increases with doping. If magnetization exists, a similar argument holds: the backward scattering Y_σ becomes ineffective at finite energy which increases with magnetization. Then both terms on the right-hand side of Eq. (3.7) are finally integrated out to make $X_\sigma(l)$ converge to some value: $K_\sigma(l)$ does not vanish so that the spin excitation spectrum is gapless.

Hereafter we always assume that magnetization is zero. Then, for spin-independent coupling, $X_\sigma = Y_\sigma$, as in the Hubbard model, the two quantities are equal at any energy scale, $X_\sigma(l) = Y_\sigma(l)$. After electron-phonon interaction is integrated out ($l > l_0$), it becomes of the form, $X_\sigma(l) = [l - l_0 + X_\sigma^{-1}(l_0)]^{-1}$. There are two possible fixed points: $X_\sigma^* = 0$ and $K_\sigma^* = 1$ if $X_\sigma(l_0)$ is positive; $X_\sigma^* = -\infty$ and $K_\sigma^* = 0$ if $X_\sigma(l_0)$ is negative. In the former, the asymptotic spin correlation is the same as in the noninteracting case ($g_{1\parallel} = 0$). In the latter, the spin part corresponds to the Luther-Emery state [13] so that the spin excitation spectrum has a gap. For $\omega = \infty$, the spin gap opens if $Y_{ph} > Y_{el}$. For $Y_{el} = 0$, the spin gap opens whenever $Y_{ph} > 0$ regardless of the phonon frequency since $X_\sigma(0)$ is negative and $X_\sigma(l)$ decreases at an increasing rate.

At half filling, the Umklapp process remains effective unless it is renormalized zero. After electron-phonon interaction is integrated out ($l > l_0$), $X_\rho(l)$ and $Y_\rho(l)$ flow on a line $X_\rho^2(l) - Y_\rho^2(l) = X_\rho^2(l_0) - Y_\rho^2(l_0)$ in the direction of decreasing $X_\rho(l)$. If $X_\rho(l_0) \geq |Y_\rho(l_0)|$, the fixed point has $X_\rho^* = \sqrt{X_\rho^2(l_0) - Y_\rho^2(l_0)}$ and $Y_\rho^* = 0$ so that $K_\rho^* \geq 1$. The superconductor correlation is dominant if $K_\rho^* > 1$. In the Holstein-Hubbard model with $Y_{ph} > Y_{el}$ and $\omega = \infty$, the initial conditions $X_\sigma(0) = Y_\sigma(0) = -X_\rho(0) = Y_\rho(0) = Y_{el} - Y_{ph}$ lead to $K_\sigma^* = 0$ and $K_\rho^* = 1$ so that it has a spin gap and degenerate singlet-superconductor and charge-density-wave correlations. It is consistent with known results for the equivalent system, namely, the attractive Hubbard model. If $X_\rho(l_0) < |Y_\rho(l_0)|$ on the other hand, $X_\rho(l)$ flows to $-\infty$ so that $K_\rho^* = 0$ and the charge excitation spectrum has a gap. This happens quite generally. For $\omega = \infty$, it applies to the SSH-Hubbard model regardless of supplementation with a forward scattering and to the Holstein-Hubbard model if $Y_{el} > Y_{ph}$. For the SSH-Hubbard model ($f = -1$ and $Y_2 = 0$), the relation $X_\rho(l) = -Y_\rho(l)$ holds at any energy scale: the charge gap always opens regardless of the phonon frequency since $X_\rho(0)$ is negative and $X_\rho(l)$ decreases at an increasing rate. For the Holstein-Hubbard model ($f = 1$ and $Y_2 = Y_1$), the charge gap appears to open as is indeed numerically supported whenever the phonon frequency is finite: the initial condition is on the line $X_\rho(0) = -Y_\rho(0)$ and the electron-phonon interaction deviates the flow to the $X_\rho(0) + Y_\rho(0) < 0$ region even if $X_\rho(0) > 0 > Y_\rho(0)$ because $Y_1(l)$ initially increases and overcomes the effect of $Y_2(l)$ then.

Consequently, three phases are possible at half filling: a charge-density-wave phase with both spin and charge gaps (SCG-CDW) with $K_\sigma^* = 0$ and $K_\rho^* = 0$; a charge-gap phase with a dominant density-wave correlation (CG-DW)

with $K_\sigma^* = 1$ and $K_\rho^* = 0$; and a spin-gap phase with degenerate singlet-superconductor and charge-density-wave correlations (SG) with $K_\sigma^* = 0$ and $K_\rho^* = 1$. The above facts of the spin and charge correlations at half filling are consistent with analytical and quantum Monte Carlo results for $Y_{\text{el}} = 0$: [14] the SCG-CDW phase always appears except for the Holstein model in the antiadiabatic limit where the SG phase appears instead. The SCG-CDW phase in the Holstein model has an ordinary charge density wave, while that in the SSH model has a bond order wave, where bond lengths and bond charge density are alternated but the charge density is uniform. Both cases have a similarity to a band insulator in the sense that they have both the spin and charge gaps. On the other hand, in the CG-DW phase, only the charge gap opens. It is similar to the repulsive Hubbard model. Without a logarithmic correction to the correlation functions, it is not clear whether the charge-density-wave order is dominant or the spin-density-wave order is dominant.

Phase diagrams at half filling are shown in Fig. 1. With $Y_{\text{el}} > 0$, Y_{ph} must be larger than a critical coupling strength to have the SCG-CDW phase. The effect of electron-phonon interaction on a spin gap depends sensitively on whether the coupling is on-site or intersite, especially when the phonon frequency is low: the critical coupling strength is much lower for the intersite coupling than for the on-site coupling. This is due to the sign factor f in the correction to the electron-phonon vertex, Eq. (3.15), and in the correction to the effective Umklapp process, Eq. (3.12). For the intersite coupling ($f = -1$), the increasing Umklapp process [$Y_\rho(l)$] strengthens the phonon-assisted backward scattering [$Y_1(l)$], contrary to the on-site coupling ($f = 1$). The Umklapp process is further strengthened by the phonon-assisted backward scattering: these two processes are constructively interfered with each other. The growing $Y_1(l)$ helps the opening of a spin gap [Eq. (3.7)] and the growth of the density-wave correlation [Eq. (3.11)]. As shown later, this difference is evident near half filling also: the intersite coupling favors the spin gap and the density-wave correlation. It is reasonable in view of the fact that, in the limit of strong on-site repulsion and small phonon frequency, the intersite coupling enables alternation of the superexchange and produces a spin-Peierls state no matter how the coupling is small. Meanwhile, the on-site coupling must be large enough to compete with the on-site repulsion to affect the system. As the phonon frequency increases, however, the difference between these two couplings becomes small. In the antiadiabatic limit, the spin gap opens for $Y_{\text{ph}} > Y_{\text{el}}$ in both cases. As a function of the phonon frequency ω , the critical coupling strength increases with ω for the intersite coupling, while it decreases for the one-site coupling.

Away from half filling, the fixed point K_ρ^* is always positive and the charge excitation spectrum is gapless since the Umklapp process is integrated out at finite energy. Therefore, four phases are possible: a gapless phase with a dominant superconductor correlation (SC) with $K_\sigma^* = 1$ and $K_\rho^* > 1$; a gapless phase with a dominant density-wave correlation (DW) with $K_\sigma^* = 1$ and $K_\rho^* < 1$; a singlet superconductor phase with a spin gap (SG-SC) with $K_\sigma^* = 0$ and $K_\rho^* > 1$; and a phase with a spin gap and a dominant charge-density-wave correlation (SG-CDW) with $K_\sigma^* = 0$ and $K_\rho^* < 1$. The DW and SG-CDW phases have a finite Drude weight, $2K_\rho^* u_\rho^*$, so that they are metallic. The DW phase appears in the doped repulsive Hubbard model. The SG-SC phase is regarded as a conventional superconductor phase since it is accompanied by a spin gap with the help of electron-phonon interaction, although a true long-range order is absent.

Far away from half filling where the Umklapp process is ineffective, a phase diagram is divided basically into the DW phase for $Y_{\text{el}} \gtrsim Y_{\text{ph}}$ and the SG-SC phase for $Y_{\text{ph}} \gtrsim Y_{\text{el}}$ (Figs. 2 and 3). For finite phonon frequency, the SC phase occupies a narrow region between the two [not shown in Figs. 2 (a) and 3 (c)] and may be an artifact of the lowest-order renormalization group approach. However, the spin correlation and the charge correlation are separated in the asymptotic limit so that there is no reason to exclude the SC phase. A phonon-assisted backward scattering tends to open a spin gap, while it enhances the density-wave correlation. To make the superconductor correlation dominant, a phonon-assisted forward scattering must overcome the backward scattering. In the continuum limit of the SSH-Hubbard model where a coupling with acoustic phonons is absent, the SG-SC phase is made possible by the supplementation with a forward scattering. [18]

Phase diagrams for the Holstein-Hubbard model are shown in Fig. 2. For very small phonon frequency ω and near half filling, the SG-CDW phase appears between the DW and SG-SC phases. In Fig. 2 (a), as the filling approaches the half ($\delta n = 0$), the boundary between the SG-CDW and DW phases goes upwards abruptly in a very close vicinity of the half filling, although it occurs too close to distinguish the boundary from the ordinate. With Y_{ph} values shown, the spin gap does not open at half filling in Figs. 2 (a) and (b). Interestingly, a spin gap is induced by doping in these two cases. The phonon-assisted backward scattering [$Y_1(l)$] is destructively interfered with the Umklapp process [$Y_\rho(l)$] so that it is not strong enough to open a spin gap at half filling for the parameters used in the figures. Upon doping, the destructive interference becomes weak and the spin gap opens. Upon further doping, the effects of $Y_\rho(l)$ and $Y_1(l)$ are overcome by the phonon-assisted forward scattering [$Y_2(l)$] in Eq. (3.11) so that $X_\rho^* > 0$, $K_\rho^* > 1$, and therefore the superconductor correlation becomes dominant. As the phonon frequency ω increases, the SG-CDW phase disappears from the higher doping side and finally goes away for a phonon frequency at a fraction of the Fermi energy. The fragility of the SG-CDW phase in the Holstein-Hubbard model is due to the fact that the cut off of the Umklapp process acts both for opening a spin gap and for strengthening the superconductor correlation. Because of retardation, the former effect becomes largest at energy of order ω , while the latter effect is independent of retardation.

This is why the SG-CDW phase is possible only for small ω . The filling dependence becomes weak with increasing ω .

The above arguments become clear when one observes the evolution of renormalized quantities with decreasing energy scale shown in Fig. 4 for the Holstein-Hubbard model. The first zero of $J_0(x)$ is about 2.4 so that the Umklapp process is cut off at about $l \sim 2$ [Fig. 4 (c)]. Before reaching the cut-off energy scale, $X_\rho(l)$ rapidly decreases [Fig. 4 (b)] and $Y_1(l)$ also decreases [Fig. 4 (d)] due to the destructive interference with $Y_\rho(l)$, which is not shown but grows exponentially. Since the phonon frequency is very small here, the electron-phonon interaction becomes effective at a much smaller energy scale. The products of an electron-phonon coupling and the corresponding phonon propagator have a peak around $l \sim 7$ and decrease exponentially after the peak [Figs. 4 (e) and (f)]. Before reaching $l \sim 7$, $X_\sigma(l)$ decreases proportionally to the inverse of l but is still positive [Fig. 4 (a)]. The magnitude of the slope of $X_\sigma(l)$ becomes large again around $l \sim 7$ and finally $X_\sigma(l)$ becomes negative: it flows to $-\infty$. Because of the destructive interference, $Y_1(l)$ is smaller than Y_1 around $l \sim 7$, and consequently $Y_1(l)D_\pi(l)$ is smaller than $Y_2(l)D_0(l)$. Therefore, $X_\rho(l)$ increases after the Umklapp process is cut off. However, the electron-phonon effect is not strong enough to make $X_\rho(l)$ positive.

Phase diagrams for the SSH-Hubbard model supplemented with a forward scattering are shown in Fig. 3. Now $Y_\rho(l)$ and $Y_1(l)$ are constructively interfered with each other. The tendency for opening a spin gap near half filling is much stronger than in the Holstein-Hubbard model, regardless of supplementation with a forward scattering. Note the difference between the scales of Figs. 2 and 3. Contrary to the Holstein-Hubbard model, as the filling deviates from the half, the constructive interference becomes weak as well as the tendency for opening a spin gap. The critical coupling strength for a spin gap is therefore an increasing function of $|\delta n|$, whose slope becomes gentle with increasing ω . Since $Y_\rho(l)$ and $Y_1(l)$ are enhanced by each other, larger deviation from half filling is necessary for $Y_2(l)$ to overcome these two to make the superconductor correlation dominant, compared with the Holstein-Hubbard model. As a consequence, the SG-CDW phase appears in a much wider region. As the phonon frequency ω increases, the interference effect becomes weak and larger electron-phonon coupling is necessary for a spin gap. Therefore, the SG-CDW phase is shifted to larger Y_{ph} values with increasing ω . However, this phase remains in the $\omega \rightarrow \infty$ limit. In this limit, the condition for a spin gap is the same as in the Holstein-Hubbard model, while the condition for a dominant superconductor correlation is different due to the sign factor f in the initial condition for $Y_\rho(0)$.

The evolution of renormalized quantities with decreasing energy scale is shown in Fig. 5 for the SSH-Hubbard model supplemented with a forward scattering. Before the Umklapp process is cut off at about $l \sim 2$ [Fig. 5 (c)], $X_\rho(l)$ rapidly decreases [Fig. 5 (b)]. Note that Y_{ph} is set at 0.1 in Fig. 5, while it was set at a much larger value of 0.4 in Fig. 4. Because of the constructive interference with $Y_\rho(l)$, $Y_1(l)$ increases when the Umklapp process is effective [Fig. 5 (d)]. Before the electron-phonon effect becomes largest at about $l \sim 5$ [Figs. 5 (e) and (f)], $X_\sigma(l)$ decreases roughly proportionally to the inverse of l [Fig. 5 (a)]. The magnitude of the slope of $X_\sigma(l)$ becomes large again around $l \sim 5$ and finally $X_\sigma(l)$ becomes negative and flows to $-\infty$. Compared with Fig. 4, the products of an electron-phonon coupling and the corresponding phonon propagator grow more rapidly and are not negligible when the Umklapp process is cut off. Therefore, the region where the electronic backward scattering decreases $X_\sigma(l)$ and the region where the phonon-assisted backward scattering decreases $X_\sigma(l)$ are not clearly distinguishable. Because of the constructive interference, $Y_1(l)$ is about twice as large as Y_1 around $l \sim 5$, and consequently $Y_1(l)D_\pi(l)$ is about twice as large as $Y_2(l)D_0(l)$. Therefore, the effects of the back and forward scatterings assisted by phonons cancel each other [Eq. 3.11] so that $X_\rho(l)$ does not change so much after the Umklapp process is cut off.

V. SUMMARY

We have studied asymptotic correlation functions of nearly-half-filled one-dimensional conductors coupled with dispersionless phonons using the boson representation of the electron fields and the lowest-order renormalization group method. On-site repulsion is considered for the electronic scattering processes. As the renormalization proceeds, the Umklapp process is initially effective even away from half filling and this causes the filling dependence of the correlation functions. We consider a phonon-assisted forward scattering which enables the superconductor correlation to be dominant. In addition, we take two types of phonon-assisted backward scatterings originating from the Holstein model and from the SSH model. They couple with both spin and charge until the energy scale reaches the phonon frequency: variation of filling modifies the spin correlation also. The variety of phases comes from the cut-off energy scale of the Umklapp process relative to that of electron-phonon interaction, which depends upon doping. The variety also comes from the interference of the Umklapp process and the phonon-assisted backward scattering, which is destructive for the Holstein-type on-site electron-phonon coupling and constructive for the SSH-type intersite electron-phonon coupling.

At half filling, a charge gap opens by the Umklapp process in most cases. A spin gap also opens if the phonon-assisted backward scattering is strong enough. Since these two processes interfere constructively for the SSH coupling, the

critical coupling strength for a charge density wave with both spin and charge gaps is weaker for the SSH-Hubbard model than for the Holstein-Hubbard model. The difference between these two models is large for small phonon frequency since the interference is effective for a wider energy range of the renormalization process. This interference effect appears also near half filling, where the Umklapp process is integrated out at finite energy so that the charge excitation spectrum is always gapless. The spin gap opens more easily by the intersite coupling than by the on-site coupling, especially for small phonon frequency. The above two processes enhance the density-wave correlation. To make the superconductor correlation dominant, the phonon-assisted forward scattering has to overcome them. It is achieved upon doping much easier for the Holstein-Hubbard model since the two negative processes interfere destructively.

Far away from half filling, a phase diagram is divided basically into the gapless metallic phase with a dominant density-wave correlation, if the on-site repulsion is stronger, and the conventional superconductor phase with a spin gap, if the electron-phonon interaction is stronger. Near half filling, we found a spin-gap metallic phase with a dominant charge-density-wave correlation between the two phases. This phase appears in a wider range for the SSH-Hubbard model supplemented with a forward scattering because of the constructive interference as mentioned above. For the Holstein-Hubbard model, it appears only for small phonon frequency, where the spin gap is induced by doping since the destructive interference is weakened as the filling deviates from the half.

For the spin-gap metallic phase, one-dimensionality is essential since the spin excitation and the charge excitation are decoupled in the asymptotic limit. The $g_{1\perp}$ process is effective only for the spin excitation and produces a gap if strong. For higher dimensions, a considerably good nesting would be necessary for a similar phase.

ACKNOWLEDGMENTS

This work was supported by Grant-in-Aid for Scientific Research on Priority Areas “Anomalous Metallic State near the Mott Transition” and “Novel Electronic States in Molecular Conductors” from the Ministry of Education, Science, Sports and Culture.

* Present address: Institute for Molecular Science, Okazaki 444, Japan

- [1] See, for example, J. Rossat-Mignod *et al.*, Physica B **169**, 58 (1991); Physica B **192**, 109 (1993); H. Yasuoka *et al.*, in *Strong Correlation and Superconductivity*, edited by H. Fukuyama *et al.* (Springer Verlag, Berlin, 1989) p.254; Physica B **199**, 278 (1994).
- [2] M. Imada, J. Phys. Soc. Jpn. **62**, 1105 (1993); **64**, 2954 (1995).
- [3] M. Imada, Physica C **185**, 1421 (1991); Physica B **188**, 822 (1993); H. Tsunetsugu *et al.*, Phys. Rev. B **49**, 16078 (1994); D. Poilblanc *et al.*, Phys. Rev. B **50**, 6511 (1994).
- [4] K. Yonemitsu, A. R. Bishop, and J. Lorenzana, Phys. Rev. Lett. **69**, 965 (1992); Phys. Rev. B **47**, 12059 (1993).
- [5] J. Zhong and H.-B. Schüttler, Phys. Rev. Lett. **69**, 1600 (1992).
- [6] H. Röder, H. Fehske, and H. Büttner, Phys. Rev. B **47**, 12420 (1993); H. Fehske, H. Röder, A. Mistriotis, and H. Büttner, J. Phys.: Condens. Matter **5**, 3565 (1993).
- [7] J. Sólyom, Adv. Phys. **28**, 209 (1979).
- [8] V. J. Emery, in *Highly Conducting One-Dimensional Solids*, edited by J. T. Devreese *et al.* (Plenum, New York, 1979).
- [9] J. Voit and H. J. Schulz, Phys. Rev. B **37**, 10068 (1988).
- [10] H. J. Schulz, Phys. Rev. Lett. **64**, 2831 (1990).
- [11] T. Holstein, Ann. Phys. (N.Y.) **8**, 325 (1959); **8**, 343 (1959).
- [12] W. P. Su, J. R. Schrieffer, and A. J. Heeger, Phys. Rev. Lett. **42**, 1698 (1979); Phys. Rev. B **22**, 2099 (1980).
- [13] A. Luther and V. J. Emery, Phys. Rev. Lett. **33**, 589 (1974).
- [14] J. E. Hirsch and E. Fradkin, Phys. Rev. Lett. **49**, 402 (1982); E. Fradkin and J. E. Hirsch, Phys. Rev. B **27**, 1680 (1983); J. E. Hirsch and E. Fradkin, Phys. Rev. B **27**, 4302 (1983).
- [15] P. A. Lee, T. M. Rice, and P. W. Anderson, Solid State Commun. **14**, 703 (1974).
- [16] K. Yonemitsu and M. Imada, Physica C (in press).
- [17] T. Giamarchi and H. J. Schulz, J. Phys. (Paris) **49**, 819 (1988).
- [18] J. Voit, Phys. Rev. Lett. **64**, 323 (1990).

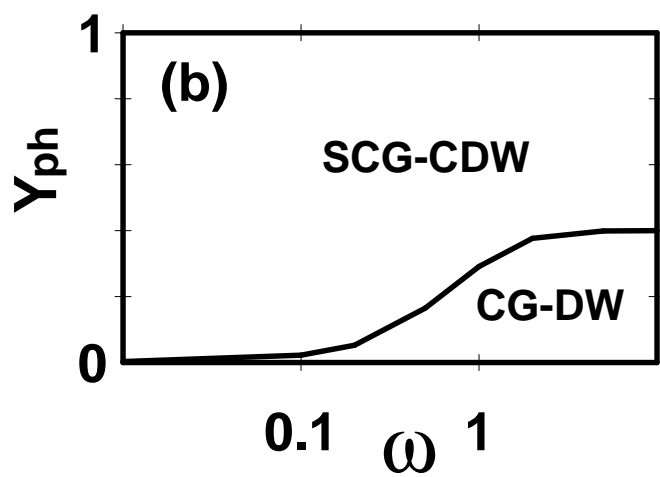
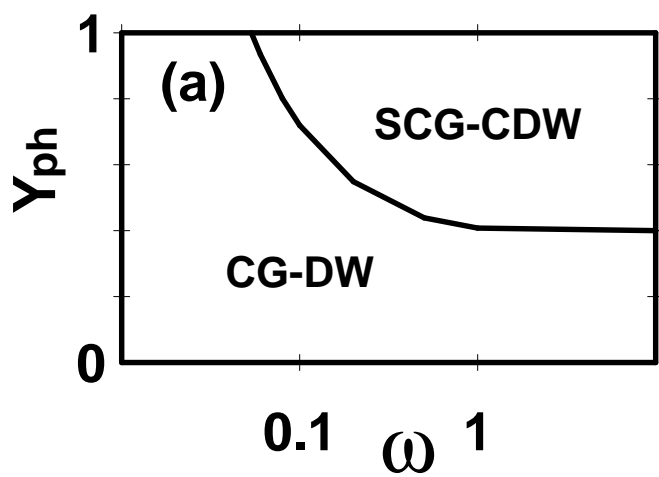
FIG. 1. Phase diagrams of (a) the Holstein-Hubbard model and (b) the SSH-Hubbard model supplemented with a forward scattering, at half filling $\delta n = 0$ and without magnetization $m = 0$. The electronic parameter is set at $Y_{\text{el}} = 0.4$.

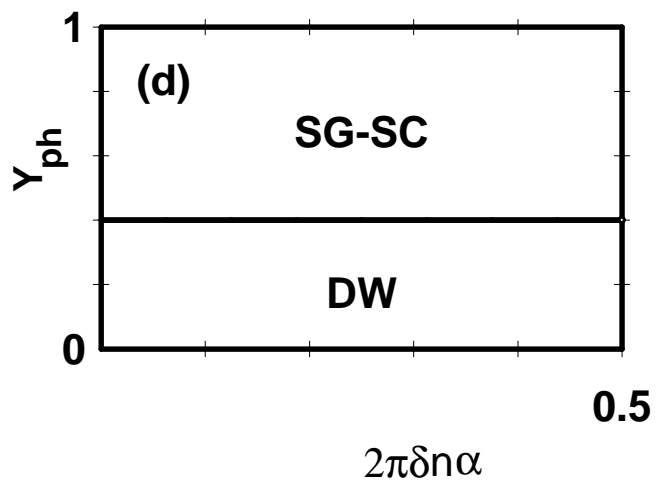
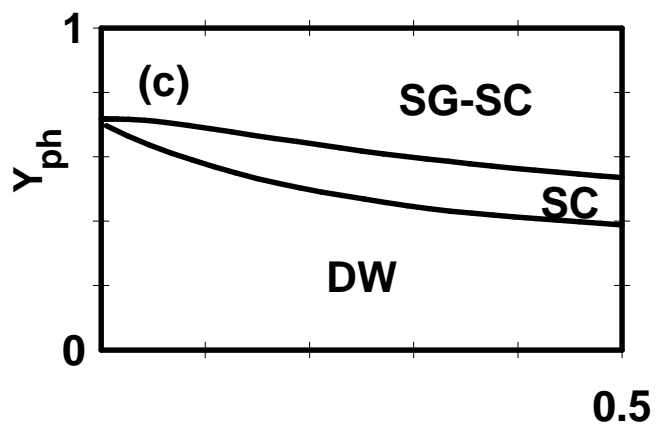
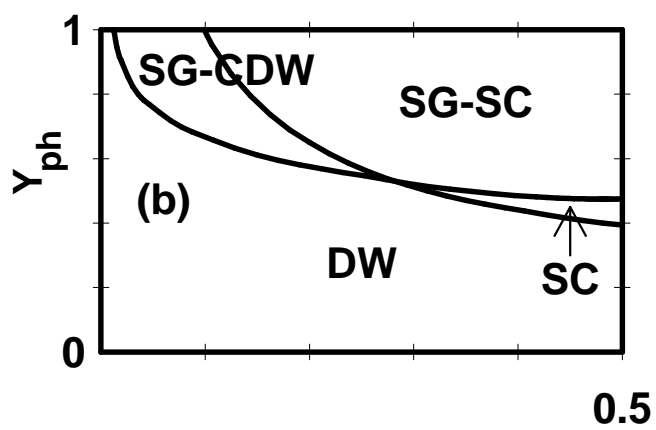
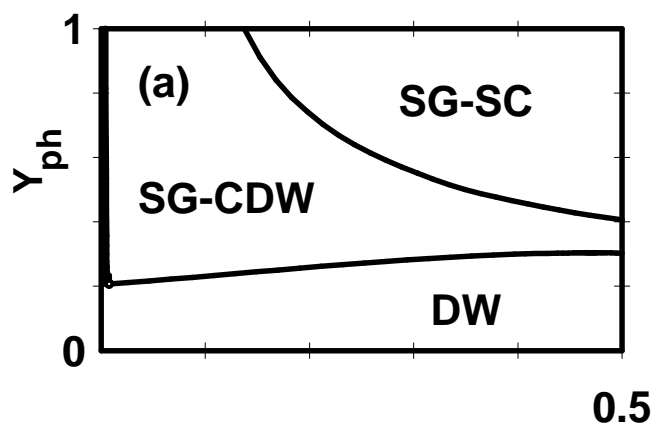
FIG. 2. Phase diagrams of the Holstein-Hubbard model for (a) $\omega = 10^{-3}E_F$, (b) $\omega = 10^{-2}E_F$, (c) $\omega = 10^{-1}E_F$, and (d) $\omega = \infty$, for $\delta n \neq 0$ (See Fig. 1 for $\delta n = 0$.) and $m = 0$. The electronic parameter is set at $Y_{\text{el}} = 0.4$.

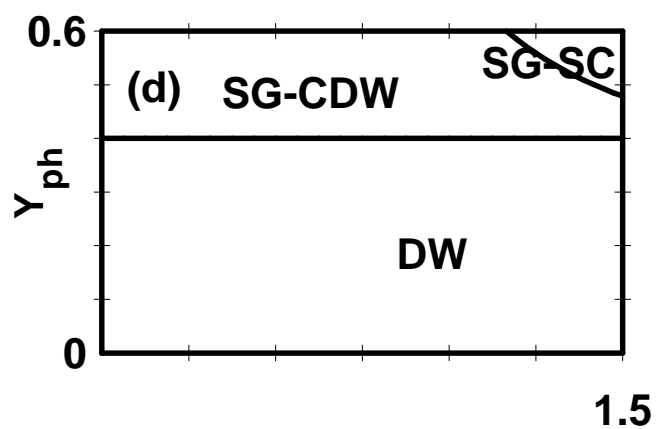
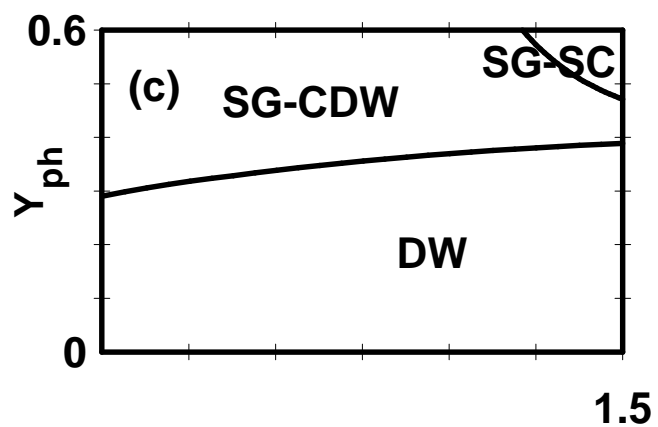
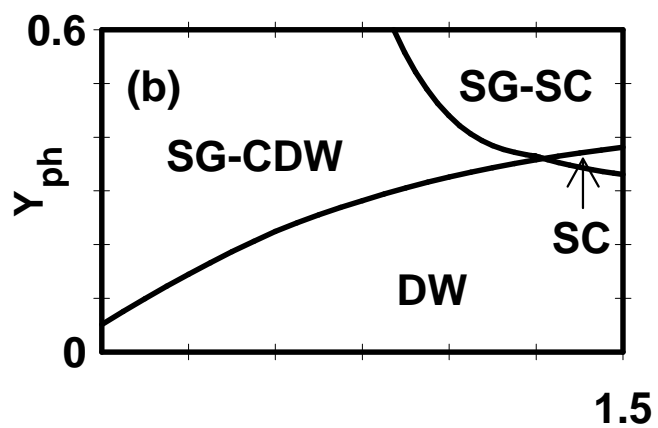
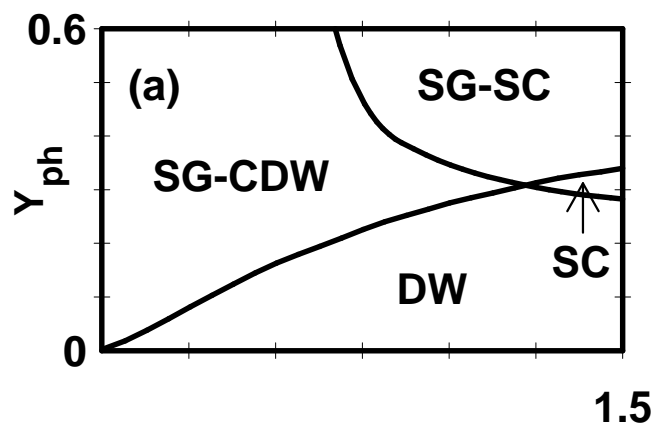
FIG. 3. Phase diagrams of the SSH-Hubbard model supplemented with a forward scattering for (a) $\omega = 10^{-2}E_F$, (b) $\omega = 10^{-1}E_F$, (c) $\omega = E_F$, and (d) $\omega = \infty$, for $\delta n \neq 0$ (See Fig. 1 for $\delta n = 0$.) and $m = 0$. The electronic parameter is set at $Y_{\text{el}} = 0.4$.

FIG. 4. (a) $X_\sigma(l)$, (b) $X_\rho(l)$, (c) $2\pi\delta n(l)\alpha$, (d) $Y_1(l)$, (e) $Y_1(l)D_\pi(l)$, and (f) $Y_2(l)D_0(l)$, in the SG-CDW phase of the Holstein-Hubbard model. Parameters are $\omega = 10^{-3}E_F$, $Y_{\text{ph}} = 0.4$, $2\pi\delta n\alpha = 0.1$, $m = 0$, and $Y_{\text{el}} = 0.4$.

FIG. 5. (a) $X_\sigma(l)$, (b) $X_\rho(l)$, (c) $2\pi\delta n(l)\alpha$, (d) $Y_1(l)$, (e) $Y_1(l)D_\pi(l)$, and (f) $Y_2(l)D_0(l)$, in the SG-CDW phase of the SSH-Hubbard model supplemented with a forward scattering. Parameters are $\omega = 10^{-2}E_F$, $Y_{\text{ph}} = 0.1$, $2\pi\delta n\alpha = 0.25$, $m = 0$, and $Y_{\text{el}} = 0.4$.







$2\pi\delta n\alpha$

